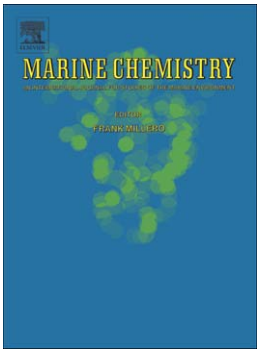

Analysis of global surface ocean alkalinity to determine controlling processes

Claudia H. Fry, Toby Tyrrell, Mathis P. Hain, Nicholas R. Bates, Eric P. Achterberg

PII: S0304-4203(15)00107-3
DOI: doi: 10.1016/j.marchem.2015.05.003
Reference: MARCHE 3246

To appear in: *Marine Chemistry*

Received date: 4 April 2014
Revised date: 29 April 2015
Accepted date: 7 May 2015

Please cite this article as: Fry, Claudia H., Tyrrell, Toby, Hain, Mathis P., Bates, Nicholas R., Achterberg, Eric P., Analysis of global surface ocean alkalinity to determine controlling processes, *Marine Chemistry* (2015), doi: 10.1016/j.marchem.2015.05.003

Analysis of global surface ocean alkalinity to determine controlling processes

Claudia H. Fry[a], Toby Tyrrell[a], Mathis P. Hain[a], Nicholas R. Bates[a,b], Eric P. Achterberg[a,c]

[a]University of Southampton, National Oceanography Centre Southampton, Southampton, UK

[b]Bermuda Institute of Ocean Sciences, Ferry Reach, Bermuda

[c]GEOMAR Helmholtz Centre for Ocean Research, 24148 Kiel, Germany

Corresponding author: C. H. Fry, Phone: +4423 8059 2037, Email: claudia.fry@noc.soton.ac.uk

Abstract

The export of calcium carbonate ($CaCO_3$) from the surface ocean is poorly constrained. A better understanding of the magnitude and spatial distribution of this flux would improve our knowledge of the ocean carbon cycle and marine biogeochemistry. Here, we investigate controls over the spatial distribution of total alkalinity in the surface global ocean and produce a tracer for $CaCO_3$ cycling. We took surface ocean bottle data for total alkalinity from global databases (GLODAP, CARINA, PACIFICA) and subtracted the effects of several processes: evaporation and precipitation, river discharge, and nutrient uptake and remineralization. The remaining variation in alkalinity exhibits a robust and coherent pattern including features of large amplitude and spatial extent. Most notably, the residual variation in alkalinity is more or less constant across low latitudes of the global ocean but shows a strong polewards increase. There are differences of ~110 µmol kg^{-1} and ~85 µmol kg^{-1} between low latitudes and the Southern Ocean and the subarctic North Pacific, respectively, but, in contrast, little increase in the high-latitude North Atlantic. This global pattern is most likely due to production and export of $CaCO_3$ and to physical resupply of alkalinity from deep waters. The use of river corrections highlights the large errors that are produced, particularly in the Bay of Bengal and the North Atlantic, if alkalinity normalization assumes all low salinities to be caused by rainfall. The residual alkalinity data can be used as a tracer to indicate where in the world's ocean most $CaCO_3$ export from the surface layer takes place, and of future changes in calcification, for instance due to ocean acidification.

Keywords

alkalinity

calcium carbonates

biogeochemical cycles

tracers

Introduction

Total alkalinity, afterwards referred to as alkalinity (*Alk*), is a measure of the acid neutralization capacity of seawater, or, more technically, the excess of proton acceptors over proton donors compared to a zero level of protons at a pH of approximately 4.3. It is measured by the stepwise addition of hydrochloric acid to determine the equivalence points of the titration curve (Dickson, 2010, 1981; Gran, 1952). Total alkalinity can be written as:

$$Alk = \left[HCO_3^-\right] + 2\left[CO_3^{2-}\right] + \left[B(OH)_4^-\right] + \left[OH^-\right] + \left[HPO_4^{2-}\right] + 2\left[PO_4^{3-}\right] + \left[H_3SiO_4^-\right] + \left[NH_3\right] + \left[HS^-\right] - \left[H^+\right] - \left[HSO_4^-\right] - \left[HF\right] - \left[H_3PO_4\right] - \left[HNO_2\right] \quad (1)$$

Measurements of two of the seawater carbonate system variables (i.e., dissolved inorganic carbon (DIC), alkalinity, pH or the partial pressure of carbon dioxide (pCO_2)), in combination with observations of temperature, salinity, silicate and phosphate concentrations, are sufficient to determine the entirety of the carbonate system. The measurement of alkalinity is particularly useful because it is conservative with respect to water mass mixing. Alkalinity is also independent of changes in temperature and pressure, unlike pCO_2, pH, and concentrations of individual chemical species (e.g. carbonate and bicarbonate) of the seawater carbonate system (Dyrssen and Sillen, 1967; Wolf-Gladrow et al., 2007).

The sea surface distribution of alkalinity is affected by several processes. These include: (1) changes in seawater dilution caused by evaporation and precipitation (Millero et al., 1998b); (2) riverine inputs of alkalinity (Cai et al., 2010; Friis et al., 2003); (3) production and export of $CaCO_3$; (4) consumption or regeneration of nutrients from primary production or respiration, respectively (Brewer and Goldman, 1976; Millero et al., 1998b; Wolf-Gladrow et al., 2007), and; (5) ventilation and upwelling of subsurface waters with high alkalinity as a result of dissolution of calcium carbonate ($CaCO_3$) (Lee et al., 2006). The inorganic carbon pump is a fundamental component of the marine carbon cycle (e.g., Hain et al. 2010;

Holligan and Robertson, 1996; Kwon et al. 2009), and may be important for sequestering organic carbon through ballasting organic matter to the deep ocean (Armstrong et al., 2002; Barker et al., 2003; Klaas and Archer, 2002). However, the magnitude of the ocean particulate $CaCO_3$ export flux is poorly known; it is currently estimated only within a large range (0.4-1.8 Pg PIC yr^{-1}; Berelson et al., 2007) and its spatial distribution is also poorly constrained. For instance, whereas satellite-based determinations of surface $CaCO_3$ concentration lead to predictions of higher calcification rates at high latitudes than at low latitudes (Balch et al., 2005), fluxes of $CaCO_3$ into sediment traps (Berelson et al., 2007) and geochemical calculations (Sarmiento et al., 2002) point to most $CaCO_3$ export occurring at low latitudes.

In this study we combined potential alkalinity (Brewer et al., 1975; Sarmiento et al., 2002) with procedures for appropriately cancelling river impacts; we subtracted all of the major processes affecting alkalinity except for (a) alkalinity removal due to formation and export of $CaCO_3$, and (b) alkalinity resupply through the upwards transport of $CaCO_3$ dissolution products from the ocean interior, hereafter jointly referred to as $CaCO_3$ cycling. Our analyses showed the large impacts of rivers on alkalinity in specific ocean regions, particularly the Bay of Bengal and the North Atlantic Ocean. The surface alkalinity data, when adjusted to take this into account, reveal greatly elevated values in the Southern Ocean and North Pacific, with well-defined gradients separating these polar regions from the rest of the ocean, which is characterized by near constant values across low latitudes. We argue that this distinct spatial pattern is consistent with its being caused by the ocean's internal $CaCO_3$ cycle, and hence that the adjusted alkalinity can be used as a tracer of $CaCO_3$ cycling.

Methods

Seawater CO_2-Carbonate Chemistry Data

Salinity, alkalinity, and nitrate data were downloaded from the GLODAP, CARINA and PACIFICA databases (http://cdiac.ornl.gov/oceans/glodap/, http://cdiac.ornl.gov/oceans/CARINA/, http://cdiac.ornl.gov/oceans/PACIFICA/). These databases were synthesized from data collected during various scientific programs since the 1980s including: (1) the Geochemical Ocean Sections Study (GEOSECS); (2) the World Ocean Circulation Experiment (WOCE); (3) the Joint Global Ocean Flux Study (JGOFS), and; (4) the Ocean and Atmosphere Carbon Exchange Study (OACES). During synthesis of each database, the data were subjected to rigorous quality control procedures. First, data flags were used to indicate the quality of the individual measurements in the cruise. Then, the data from different cruises were compared using the assumption that deep values have low spatial and temporal variability, and therefore that adjacent data points from different cruises should have similar values. Data with a lower than acceptable quality were removed and small biases in cruises adjusted (Key et al., 2010, 2004; Millero et al., 1998a; http://cdiac.ornl.gov/oceans/PACIFICA/). For this study, we used only bottle data rather than any gridded products. The surface ocean was defined as shallower than 30 m at latitudes greater than 30°, and shallower than 20 m at latitudes less than 30°, as in previous studies (Lee et al., 2006). We included only open ocean data (seafloor depth > 200 m) in our analysis. Data from the Arctic and Mediterranean seas were excluded. Thus this study excluded shelf seas, shallow coastal seas, and enclosed seas.

Analysis of Process Contributions

Controls on surface alkalinity were analyzed using in-situ alkalinity data together with associated hydrographic properties. The impacts of various processes on the spatial distribution of alkalinity in the surface ocean were calculated from related variables. The

effects of freshwater fluxes (evaporation, precipitation, river discharge) were quantified based on salinity, and biological fluxes of nutrients calculated using nitrate data.

Following the subtraction of each major process that affects alkalinity, the overall distribution of alkalinity was recalculated and reanalyzed to assess whether it had become more coherent (i.e., less scatter among nearby observations). For each basin, the data were binned by 5° latitude, and the mean and standard deviation of each bin was calculated. To create a dimensionless statistical variable, the value of which could be compared to other hydrographic variables, the mean standard deviation for each basin was divided by the range of the bin means for that basin. The same statistical approach was undertaken for nitrate, phosphate, and silicate. As an example, for nitrate in the Atlantic, the metric for the average spread of the data cloud is calculated as:

$$M_{NO3,ATL} = \frac{\left(\frac{1}{36}\sum_{i=1}^{i=36}\sigma(NO3_i^{ATL})\right)}{\left(\max\left(\overline{NO3_i^{ATL}}\right) - \min\left(\overline{NO3_i^{ATL}}\right)\right)} \quad (2)$$

where $\overline{NO3_i^{ATL}}$ and $\sigma(NO3_i^{ATL})$ are the mean and standard deviation of the nitrate values in the i'th Atlantic bin.

After subtraction of all processes except the $CaCO_3$ cycle, the final surface distribution of alkalinity was assessed as a tracer of $CaCO_3$ cycling.

Results

Evaporation and Precipitation

Figures 1a, b and c show the measured surface ocean alkalinity distributions in the Atlantic, Indian and Pacific basins as a function of latitude, with colors indicating salinity. The relative mean standard deviations of the 5° bins are shown in Table 1. For all three basins, the most

obvious features of the datasets are the local maxima of alkalinity around 30°N and 20°S, which correspond to the centers of the subtropical gyres. These peaks contrast with much lower values (up to 400 µmol kg^{-1} lower) near the equator and in the polar ocean regions.

The consistent elevation of alkalinity in the subtropical gyres is caused principally by the hydrological cycle driving substantial excess evaporation over precipitation in these regions. Net evaporation concentrates substances dissolved in seawater, as freshwater is lost to the atmosphere and solutes are left behind. Conversely, net precipitation dilutes seawater, as relatively pure water is added. Because alkalinity is a weighted sum of different dissolved constituents (equation 1), its concentration rises and falls proportionally with salinity.

Variations in salinity are used to calculate the balance between the effects of evaporation and those of precipitation. Figure 2a shows alkalinity plotted against salinity in the global surface ocean. Pearson's correlation coefficients (r) were 0.94 in the Atlantic Ocean, 0.87 in the Indian Ocean, 0.92 in the Pacific Ocean, and 0.94 when data from all the oceans were combined. These strong correlations are consistent with evaporation and precipitation being responsible for most of the variation in alkalinity.

The effects of evaporation and precipitation can be removed from alkalinity by converting each alkalinity measurement, Alk_m, to its expected value at a salinity (S) of 35, i.e. by normalizing each value to a salinity of 35 (Postma, 1964; Millero et al., 1998b):

$$Alk_1 = \frac{Alk_m}{S} \times 35 \qquad (3)$$

Figure 2b shows that the major correlation between salinity and alkalinity, especially at high salinities, is removed using equation 3. Equation 3 successfully negates the effect of the hydrological cycle, eliminating the elevated alkalinity of the subtropical gyres and the local minima of alkalinity along the equator, thereby resulting in fairly constant low-latitude

surface Alk_1 (Figure 1d, e and f). As can be seen in Table 1, the variability of alkalinity relative to its overall range is reduced in all three basins following removal of evaporation and precipitation effects.

Riverine Input

Although salinity normalization reduces the spatial variability in alkalinity in the subtropics, many features still remain (Figure 1d, e and f). For instance, in the north Indian Ocean there are two different regimes of alkalinity at a similar latitude: the Bay of Bengal is characterized by lower observed alkalinity and salinity, but by a higher normalized alkalinity than the Arabian Sea. There is also a significant high anomaly in normalized alkalinity at 8°N in the Atlantic Ocean, and several high anomalous groups between 40°N and 60°N in the North Atlantic. In both oceans these areas also correspond to low observed salinity (compare Figure 1a and Figure 1d, and Figure 1b and Figure 1e; salinity-normalized alkalinity values that are more than 20 µmol kg^{-1} from the 5° latitude running mean are indicated in red).

Low salinity is not always produced by rainfall, but can also be produced by sea-ice melt or by inputs of river water. In non-polar waters, the obvious likely cause of the overcorrection from the salinity-normalization is therefore river input. Based on a global analysis of volume of river water received, the ocean areas most likely to be affected are the Arctic Ocean, the Bay of Bengal, the Labrador Sea, the Amazon River and Congo River plumes in the Atlantic, and the South China Sea (Kang et al., 2013).

Friis et al. (2003) found that misleading results are produced if equation 3 is used to normalize alkalinity to salinity in ocean regions receiving river outflows. Equation 3 assumes that freshwater discharged by rivers (i.e., zero salinity) also has zero alkalinity, which is not the case since many rivers have substantial concentrations of alkalinity, in particular those draining limestone catchments (Cai et al., 2010). In marginal seas, the y-intercept of the

relationship between alkalinity and salinity usually (although not always, see Jiang et al. 2014) corresponds to the alkalinity of the river end member, Alk_r, because, assuming conservative mixing, this is the value of alkalinity when the salinity is negligible (river water). Following Friis et al. (2003), we used equation 4 to account for river input:

$$Alk_2 = \frac{Alk_m - Alk_r}{S} \times 35 + Alk_r \quad (4)$$

The peak at 8°N in the Atlantic basin is close to the South American continent; therefore, it is likely that these data have been influenced by the Amazon River, and examination of the geographical locations of the anomalous points confirms that they lie in the general area of the Amazon outflow plume. The water from the mouth of the Amazon River has an Alk_r value of around 300 μmol kg^{-1} (Cooley et al., 2007; Cooley and Yager, 2006). When the salinity normalization by Friis et al. (2003) (equation 4, with Alk_r = 300 μmol kg^{-1}) is applied for the region between the latitudes of 5 and 10°N and west of 45°W in the Atlantic basin, the anomalous peak at 8°N is eliminated (Figure 1g versus Figure 1d).

Figure 3 shows that the anomalously high normalized alkalinity values in the region between 40°N and 60°N in Figure 1a are geographically situated close to the Labrador coast. Millero et al. (1998b) also found an anomalous area in salinity-normalized alkalinity in the vicinity of the Labrador Sea. Cai et al. (2010) suggested that the Labrador Current is the source of the anomalous alkalinity rather than local runoff. This implies that the intercept of the salinity-alkalinity relationship will not agree with the alkalinity for local continental runoff. The y-intercept of the Labrador Current, Alk_r, equals 1124 μmol kg^{-1}, which is close to the composite of the runoff from the six largest Arctic rivers of approximately 1100 μmol kg^{-1} (Cooper et al., 2008). A revised alkalinity was calculated for the Atlantic Ocean (Figure 1g) where an Alk_r = 300 μmol kg^{-1} was used for the region between 5°N and 10°N and west of

45°W to correct for the Amazon River plume, and Alk_r = 1100 µmol kg^{-1} in the Labrador Sea inflow area (defined as north of 40°N and west of 30°W). Comparing Figure 1g to 1d, the Atlantic Ocean has fewer anomalously high points and a lower standard deviation (Table 1). However, some of the points in the Labrador Current are now lower than the mean and appear to have been overcorrected; this is most likely due to the presence of anomalous surface water in the area, of unknown origin, which has previously been found to have a much lower Alk_r of 273 µmol kg^{-1} (Cai et al., 2010).

Figure 3 also shows that the high salinity normalized alkalinity values in Figure 1e come from the Bay of Bengal. The mean measured alkalinity in the outflow of the Ganges-Brahmaputra is 1106 µmol kg^{-1} (Galy and France-Lanord, 1999). Using this as the value of Alk_r in the Bay of Bengal area (defined as the part of the Indian Ocean north of 5°N and between 80°E and 94°E) led to an overcorrection of the higher branch in the north Indian Ocean (Figure 4). When river alkalinity based on modeling of annual river runoff and basin lithology and weathering (Alk_r = 840 µmol kg^{-1}; Amiotte Suchet et al., 2003) was used instead of direct measurements, the anomaly in the north Indian Ocean was successfully corrected (Figure 1h). The Ganges-Brahmaputra alkalinity (Bates et al., 2006) and water (Kang et al., 2013) fluxes vary seasonally; the differences between modeled and observed Alk_r may therefore be down to seasonal differences.

After removing the salinity normalization error caused by large river inputs (summarized in Table 2), the remaining alkalinity distribution is as shown in Figures 1g, h, i. The standard deviations of those basins where changes were made are improved (lower), as shown in Table 1.

Nutrient Uptake and Remineralization

Biological consumption and production of nitrate cause an equivalent change in alkalinity (Brewer and Goldman, 1976; Goldman and Brewer, 1980) despite the fact that nitrate does not appear in the formal definition of alkalinity (equation 1). This is because nitrate consumption/production is stoichiometrically tied to the removal/addition of nitric acid, and the H^+ removed/added does affect alkalinity. A reduction in nitrate concentration has to be matched with an increase in alkalinity of the same magnitude in order to maintain the balance of charge in the water. Therefore, nitrate consumption and denitrification increase alkalinity, and nitrate generation (nitrification) following remineralization decreases alkalinity. Other species such as sulphate and phosphate have similar effects on alkalinity (Wolf-Gladrow et al., 2007).

The alkalinity changes arising from the biological cycling of nitrate are often accounted for in the concept of potential alkalinity, *pAlk* (e.g. Brewer et al., 1975; Sarmiento et al., 2002), where the sum of the nitrate and alkalinity concentrations is normalized to a salinity of 35. Wolf-Gladrow et al. (2007) calculated changes in alkalinity from primary productivity, taking into account the proportional uptake of other ions such as phosphate and sulphate. They suggested that the impact of phytoplankton growth on alkalinity should be calculated by multiplying changes in the nitrate ion concentration, $[NO_3^-]$, by a factor of 1.36. Hence:

$$pAlk = \frac{Alk_m + 1.36 \times NO_3^-}{S} \times 35 \tag{5}$$

Figures 1j, k, l show the resulting patterns in alkalinity, after variations in nutrient concentration have also been taken into account, using:

$$Alk_3 = \frac{Alk_m - Alk_r + 1.36 \times NO_3^-}{S} \times 35 + Alk_r \tag{6}$$

Incorporation of the effects of creation and remineralization of biological matter increases the average offset between low latitudes and high latitudes from ~75 µmol kg^{-1} to ~100 µmol kg^{-1}. This is because the Southern Ocean and subarctic North Pacific are both regions of the global ocean with high surface nitrate concentrations.

Pattern in the Residual Alkalinity

After excluding the effects of nutrients on alkalinity, there is a fairly uniform alkalinity of ~2300 µmol kg^{-1} in the low-latitude surface oceans (30°N-30°S). Table 1 shows that with every additional step the width of the data cloud relative to the overall range of the data has decreased. This suggests that the effects of processes causing variation have been successfully removed. The remaining variation is comparable to that of the major nutrients (Table 1). This would be expected if Alk_3 and the nutrients are mainly controlled by uptake to form new phytoplankton, and returned through exchange with deep water following export and remineralization.

To examine the remaining large-scale spatial pattern in the distribution of surface alkalinity. We define the new tracer *Alk** to have a low latitude concentration of ~ 0 µmol kg^{-1} (i.e. $Alk^* = Alk_3 - 2300$ µmol kg^{-1}). Thus, the value of Alk* corresponds to the "excess alkalinity" compared to the tropical and subtropical surface ocean. It can be seen (Figure 1m, n and o) that *Alk** values in the high-latitude regions of the North Pacific and Southern Ocean are strongly elevated by ~85 µmol kg^{-1} (north of 55°N) and ~110 µmol kg^{-1} (south of 75°S), respectively. Interestingly, there is no correspondingly large elevation of *Alk** in the high-latitude North Atlantic: the average *Alk** value at 55°N in the Atlantic is only 24 µmol kg^{-1}. Notably, the low-latitude to polar ocean increases in alkalinity are somewhat weaker when nutrient cycling effects are not included; the same overall geographic distribution is obtained

but with smaller magnitude differences (e.g., compare Alk_2 in Figure 1g, h, and i to Alk_3 in Figure 1j, k, and l).

Discussion

Comparison to Other Approaches

In this paper we have derived a tracer for $CaCO_3$ cycling in the surface ocean based on observed alkalinity and removal of other influences, including: (1) freshwater evaporation and precipitation; (2) inputs of river water containing alkalinity at negligible salinity; and (3) biological cycling of nutrients.

The procedure we employed is an extension of the potential alkalinity concept (Brewer et al., 1975; Rubin and Key, 2002; Sarmiento et al., 2002; Wolf-Gladrow et al., 2007); however, it also includes a correction for the influence of high-alkalinity rivers (Cai et al., 2010; Friis et al., 2003). Our analysis shows that high-alkalinity rivers can influence large ocean areas (e.g. Figure 1g versus Figure 1d). We show that the North Atlantic Ocean and the Bay of Bengal are strongly influenced by river derived alkalinity inputs. We expect that with incorporation of more marginal regions (Key et al., 2010), such as the South China Sea (Kang et al., 2013), and more seasonal data, river alkalinity will become an increasingly important part of alkalinity process analysis. Our *Alk** tracer for surface waters also bears some resemblance to that of 'excess' alkalinity (Feely et al., 2004, 2002; Sabine et al., 2002), which was developed to quantify $CaCO_3$ dissolution rates along isopyncal surfaces. We use *Alk** to constrain surface $CaCO_3$ cycling (as defined here) as a whole, as opposed to specifically targeting the dissolution of $CaCO_3$ at depth. This gives a tracer that is similar to nutrient tracers and can be used to investigate biological production in a similar way to that of nutrients.

In this paper we revisit some of the same issues as those of an earlier study (Millero et al., 1998b), which used salinity-normalized alkalinity. Some of the large-scale patterns we find were also noted previously by Millero et al. (1998b), but are now more clearly defined and can be accepted with greater confidence, based on the improved analysis techniques and larger quantity of data used in this study.

*Accounting for the Patterns in Alk**

The surface field of *Alk** is distinct from the actual alkalinity observations (first and last rows of Figure 1). Eliminating the effects of the hydrological cycle, rivers and nutrient cycling reveals coherent basin-scale patterns in *Alk** that are not apparent in Alk_m. We argue that these patterns directly reflect the imprint of the ocean's $CaCO_3$ cycle, or in other words that the patterns in *Alk** are maintained by the inorganic carbon pump acting against ocean overturning and mixing. As with dissolved nutrients, *Alk** is reduced when and where biological precipitation of $CaCO_3$ occurs. The $CaCO_3$ sinks from the mixed layer into the deep ocean, where $CaCO_3$ undersaturation causes it to dissolve and increase the deep *Alk** concentration. Large-scale ocean circulation brings the deep water back to the surface, producing higher *Alk** concentrations in the polar ocean surface of the Southern Ocean and the North Pacific.

High Alk in High-latitude Oceans*

In line with previous interpretations (Key et al., 2004; Lee et al., 2006; Millero et al., 1998b; Sabine et al., 2002), we identify the source of increased salinity-normalized alkalinity at high latitudes as supply of excess alkalinity from deep waters. High alkalinity at depth can be transferred to high-latitude surface waters either through upwelling, transfer along isopycnals outcropping at high latitudes, and/or entrainment of deep waters into the mixed layer during deep winter mixing. The individual contribution of these physical processes to high *Alk** in

surface waters may vary among distinct regions, and subsurface waters are also expected to contain variable concentrations of excess alkalinity to be brought to the surface in different parts of the world's ocean (see explanation for low North Atlantic *Alk** below). In addition, the strength of these sources may vary seasonally; for example, deep winter mixing may cause higher *Alk** in an area during winter with subsequent lower levels in summer.

We attribute the relatively low *Alk** values in the subarctic North Atlantic to the low *Alk** values at depth in this region. To illustrate the reason for this exception, we calculated *Alk** along a vertical ocean section from the North Atlantic, through the Southern Ocean and into the North Pacific (Figure 5). From this interior ocean view of the alkalinity anomaly, it is clear that the high surface *Alk** values of the Southern Ocean and subarctic North Pacific directly correspond to elevated *Alk** in subsurface waters, whereas the low surface *Alk** values of the subarctic North Atlantic are above low *Alk** of the North Atlantic Deep Water (NADW) . The difference between the regions can be attributed in part to differences in the ages of the deep waters underlying the various regions. The main source of NADW is surface water that was recently subducted following poleward transport from lower latitudes (e.g., Lozier, 2012).Therefore, the subpolar North Atlantic surface and NADW both inherit a low *Alk** from the Atlantic meridional overturning circulation passing through the low-latitude surface Atlantic, where *Alk** is also low. Because of the small vertical gradient, winter mixing in the high-latitude North Atlantic, although penetrating to considerable depths (hundreds of meters; de Boyer Montegut et al., 2004), produces little increase in surface *Alk**. Alkalinity distributions along similar sections to Figure 5 have been explained (Pardo et al. 2011; Vázquez-Rodríguez et al. 2012) using the concept of pre-formed alkalinity, which is the alkalinity at the point subducting water loses contact with the atmosphere. As the high-latitude North Atlantic is a deep-water formation region, the low *Alk** determines the pre-

formed value, with $CaCO_3$ dissolution increasing *Alk** as NADW travels southward through the Atlantic Ocean.

The subarctic North Atlantic contrasts with the subarctic North Pacific, where winter mixing, although not reaching to such great depths (up to about 150 m on the eastern side and 250 m on the western side; Ohno et al., 2009), does reach high *Alk** subsurface waters (50-200 µmol kg^{-1}) because of the strong vertical gradients (Figure 5). In the Southern Ocean the situation is more complicated but there is no formation of deep water from low-latitude surface water, and deep water consequently has high *Alk** (Figure 5). Furthermore, wind-driven upwelling introduces high *Alk** water to the surface from greater depths than in other parts of the world's ocean (Toggweiler and Samuels, 1995).

Low Alk in Low-latitude Oceans*

To the degree that the global $CaCO_3$ cycle is near internal balance, the net upwards transport of dissolved *Alk** across the main thermocline must equal the global downwards $CaCO_3$ rain across the thermocline. Low *Alk** values in the tropical and subtropical surface oceans are therefore understood as resulting from $CaCO_3$ formation and export leading to removal of *Alk** from surface waters, together with an absence of significant replenishment from deep water. The data show surprisingly similar values in all basins at low latitudes (averages of 2297, 2294 and 2305 µmol kg^{-1} between 30°S and 30°N in the Atlantic, Indian and Pacific Oceans, respectively).

Similarity of Residual Alkalinity Distribution to Nutrients

Attributing the *Alk** patterns to $CaCO_3$ cycling is further supported by the partial resemblance between the latitudinal distributions of *Alk** and those of the nutrients: nitrate, phosphate and silicate (Figure 6). Concentrations of all are depleted in the subtropical surface ocean due to

biological use. All four exhibit maxima in concentrations at high latitudes in the Southern Ocean and North Pacific, but a more modest increase in the high-latitude North Atlantic.

There are however some differences. For example, in contrast to nitrate and phosphate, neither silicate nor alkalinity exhibit large increases in concentration in the north Indian Ocean or in the eastern Equatorial Pacific. This may reflect different remineralization depths (nitrate and phosphate are both returned to solution at much shallower depths than silicate from opal rain or alkalinity from $CaCO_3$ rain; Schlitzer, 2000) and the source of the water. Alternatively, it may be co-occurrence of upwelling and intensive $CaCO_3$ production, which would not be identified in our tracer. A previous study has found salinity-normalized alkalinity to be ~40 μmol kg^{-1} higher in upwelled water in the eastern Equatorial Pacific (Millero et al., 1998b).

A second difference is apparent when comparing the latitude at which all four variables decrease to negligible levels when moving northwards away from Antarctica. Concentrations of silicate have declined almost to zero by about 50°S, whereas *Alk**, nitrate and phosphate are all still significantly elevated at this latitude and it is not until about 40°S that all three decline to near zero (Figure 6). One explanation of this feature could be the greater competitive success of silicifiers in the Southern Ocean, with diatoms blooming and depleting silicate concentrations further south than other phytoplankton. Therefore, silicate is used up further south than nitrate, phosphate, and *Alk** (Sarmiento et al., 2004). Pronounced yearly blooms of coccolithophores are seen in satellite observations in the region of the subantarctic zone (about 50ºS to 40ºS) of the Southern Ocean (Iglesias-Rodriguez et al., 2002). This feature has been termed the "Great Calcite Belt" (Balch et al., 2011) and may be responsible for one third of global export of $CaCO_3$ (Jin et al., 2006). However, in order to

identify more confidently where $CaCO_3$ production and export take place, the tracer should ideally be used in conjunction with an ocean circulation model.

Overall, the nutrient-like distribution of *Alk** is consistent with the expected bahaviour of a tracer of $CaCO_3$ production and dissolution.

Similarity of Residual Alkalinity to Residual Calcium

Results from a second and independent method of constraining $CaCO_3$ cycling can be compared to those from the *Alk** method. The concentration of calcium ions (measurable to a precision of about ± 3 µmol kg^{-1}; Olson and Chen, 1982) is also directly affected by dilution and concentration, production and dissolution of $CaCO_3$, and river input of $CaCO_3$, but not biological cycling processes affecting alkalinity. After salinity normalization, the surface ocean has a slightly lower concentration of calcium than at depth, due to the $CaCO_3$ pump (Milliman et al., 1999). The ratio of Ca^{2+} to salinity has previously been demonstrated as a tracer of $CaCO_3$ cycling in the South China Sea (Cao and Dai, 2011), and salinity-normalized calcium concentration (NCa) agrees well with salinity-normalized alkalinity as a tracer of $CaCO_3$ cycling in deep waters of the Sea of Okhotsk (Pavlova et al., 2008). Both Ca-based and Alk-based tracers of $CaCO_3$ cycling are made less effective in the deep ocean because low-temperature hydrothermal vents are an alternative source of calcium (Chen, 2002; de Villiers, 1998; de Villiers and Nelson, 1999).

If $CaCO_3$ cycling is the dominant influence over both *Alk** and NCa then we predict the following NCa patterns in surface waters: (1) it should be relatively invariant across low-latitude oceans; (2) it should differ by about 40 µmol kg^{-1} (ΔCa from $CaCO_3$ formation/ dissolution = 0.5 * Δ*Alk**) between low and high latitudes in the North Pacific; (3) it should be about 55 µmol kg^{-1} higher in the high-latitude Southern Ocean than in low-latitude

regions; and (4) it should not vary greatly between low and high latitudes in the North Atlantic.

Relatively few calcium data currently exist with which to test these predictions, and what does exist is only partly compatible with them. Chen (2002) reported calcium concentrations along 150°W in the North Pacific from 8 to 55°N: highest NCa values along the transect were observed at the highest latitudes (north of 45°N); however, an unexpectedly high degree of low-latitude variability (> 20 μmol kg^{-1}) is also apparent in the data. NCa values from the Weddell Sea are approximately 70 μmol kg^{-1} higher than values from the low-latitude Pacific Ocean (Chen, 2002). Tsunogai et al. (1973) found a poleward increase of the calcium to chlorinity ratio along 170°W.

Some Uncertainties and How They Might be Reduced in Future Work

Here, we consider sources of uncertainty in *Alk** and, where applicable, how they might be minimized in future work. The geographical differences in *Alk** are large compared to the accuracy of alkalinity measurements (~3 μmol kg^{-1}, Dickson et al., 2003), which can thus be ruled out as a cause. There is some bias in the collection of data, with surveys in high latitude regions occurring more frequently during summer months because of weather considerations (Key et al. 2004). Because alkalinity resupply to the surface by vertical mixing changes with season including more wintertime data could increase high-latitude *Alk** values, thereby further increasing the contrast to the low-latitude surface that has no seasonal bias.

Some local river flows need to be considered when using open ocean data (Cai et al., 2010), as demonstrated here by the wide-scale influences of river derived alkalinity inputs to the Bay of Bengal and Atlantic Ocean. Kang et al. (2013) identified the South China Sea as another area affected by river inputs of alkalinity; however, we made no adjustment because of a lack

of seawater data for the region. When using river alkalinity data to correct for river influences in offshore regions, it should be kept in mind that differences in riverine input alkalinity can be caused by non-conservative estuarine changes to fluxes such as from anaerobic processes occurring in the river delta (Hu and Cai, 2011), as has been recorded in river systems (Cai and Wang, 1998; Wong, 1979). Also, simply fitting a line to alkalinity-salinity data is not always a reliable method of determining the river end-member alkalinity (Jiang et al., 2014). Further research is required on alkalinity in the outflows of major rivers and the penetration of their effects into the open ocean.

$CaCO_3$ cycling is the dominant influence on the residual alkalinity, but other processes will also have smaller effects. Some second-order or locally important processes for alkalinity have not been calculated and removed from *Alk**. These include anaerobic remineralization processes (denitrification and sulphate reduction could affect the surface waters in coastal regions), formation and destruction of sea-ice and ikaite (e.g. Rysgaard et al., 2013; 2012), organic alkalinity (Bradshaw and Brewer, 1988), and nitrogen-fixation (Wolf-Gladrow et al., 2007). Development of techniques for the removal of these influences would further improve *Alk**. Many of these processes, such as the impact of organic alkalinity, the formation and destruction of sea-ice, and anaerobic remineralization are of greater importance in areas that are not included in this study, such as in coastal regions and the Arctic Ocean.

There is a limit to the accuracy with which the magnitude of calcification can be determined in river affected ocean from an alkalinity-based tracer. This is because the order in which calcification and mixing take place (which is not usually known) affects the resulting change in alkalinity (Jiang et al, 2014). This can be important when two bodies of water mix, for example when seawater mixes with river water. If calcification occurs (A to b in Figure 7) before the mixing with river water (b towards R in Figure 7), then the final alkalinity value (c

in Figure 7) differs from that when mixing occurs before calcification (A to d to e in Figure 7). Equation 6 for Alk* assumes calcification occurs before mixing and so if they occur in the opposite order then the inferred amount of calcification would be inaccurate. But, from calculations on our dataset when we assumed a reversed order, the difference is within the current measurement error of alkalinity (<3 μmol kg^{-1}). In addition, *Alk** is not completely conservative because of salinity-normalization. When two water bodies mix, the calculated *Alk** of the mixture is not exactly equal to the weighted average of the source *Alk** values, although the difference is usually small (<5%).

We can quantify the propagated measurement uncertainty in *Alk** from the definition of Alk_3 (equation 6), which in absolute terms has the same uncertainty as *Alk**, and from rules for propagating uncertainties through calculations (Taylor, 1982). The uncertainty in *Alk** values is calculated using equation 7 and measurement uncertainties of: alkalinity, ΔAlk_m, 3 μmol kg^{-1} (Dickson et al., 2003); salinity, ΔS, 0.0015 (Perkin and Lewis, 1980), and nitrate, ΔNO_3^-, 0.2 μmol kg^{-1} (Aminot and Kirkwood, 1995). Errors in river input measurements were not considered as most of the dataset is not affected by the adjustment. The estimated overall uncertainty of *Alk**, $\Delta Alk^*$is 3.02 μmol kg^{-1}. The uncertainties are thus small compared to the large latitudinal differences in *Alk**.

$$\Delta Alk^* = \frac{35\times(Alk_m + 1.36\times NO_3^-)}{S}\times\sqrt{\left(\frac{\Delta S}{S}\right)^2 + \frac{(\Delta Alk_m)^2 + \left(1.36\times\Delta NO_3^-\right)^2}{\left(Alk_m + 1.36\times NO_3^-\right)^2}} \quad (7)$$

*Potential Uses of Alk**

This new tracer of surface $CaCO_3$ cycling is likely to be useful in a number of ways. The first example is in the calculation of $CaCO_3$ export fluxes.

Where horizontal and vertical water fluxes are known, they can be combined with *Alk** gradients to estimate the rate of loss of calcium carbonate (export flux) from the mixed layer. Figure 8 shows the fluxes that affect *Alk** of the low-latitude surface water in the Atlantic. Supply of *Alk** through mixing across the thermocline and equatorial upwelling is assumed negligible as this process does not contribute to the observed surface ocean pattern. Average Alk_3 is 2299 µmol kg^{-1} at 30°S ($Alk^*_{S.Atl.}$ = -1) and 2289 µmol kg^{-1} at 30°N ($Alk^*_{N.Atl.}$ = -11) (Figure 1j). If NADW formation (F_{NADW}) and the surface Ekman water flux from the Southern Ocean (F_{Ekman}) are equal at 18±3 Sverdrups (Talley et al., 2003), then the rate of *Alk** vertical export, Q_{Atl}, from the Atlantic Ocean can be calculated as a function of the water flux and the decline in alkalinity in transit:

$$\begin{aligned} Q_{Atl} &= F_{Ekman} \times Alk^*_{S.Atl.} - F_{NADW} \times Alk^*_{N.Atl.} \\ &= F_{Ekman} \times (Alk^*_{S.Atl.} - Alk^*_{N.Atl.}) \end{aligned} \quad (8)$$

This produces an estimated $CaCO_3$ export of ~0.03 Pg PIC yr^{-1} with an uncertainty of ±0.01 based on the uncertainty in the Ekman flux. This value is significantly lower than previous estimates of Atlantic $CaCO_3$ production (0.11-0.69 Pg PIC yr^{-1}; see Table 3) and an Atlantic-wide estimate of $CaCO_3$ dissolution in deep water (0.13 Pg PIC yr^{-1}; Chung et al., 2003). Our value suggests that rather little calcification takes place in the upper mixed layer of the Atlantic. Our estimate is of export rather than production but dissolution is probably minor in the supersaturated surface ocean and so the two are probably similar. The discrepancy with other estimates could potentially be reconciled if calcification is primarily taking place in deeper parts of the euphotic zone, i.e. below the surface mixed layer (Poulton et al., 2006) or further south in the Atlantic sector of the Southern Ocean (Figure 1j). Another explanation is that equatorial upwelling does supply *Alk** and it is used too quickly to be seen in the surface concentrations. We suspect that the largest uncertainty in our calculation stems from the

assumption that the only flows are NADW and associated net flow through the tropical Atlantic box, which is an oversimplification.

*Alk** could also be used to analyze the spatial distribution of $CaCO_3$ export. Calculation of *Alk** on different depth and/or density levels may help resolve the question about where in the oceans most $CaCO_3$ is produced and exported. In the surface layer at least, the steepest horizontal gradients in *Alk** are at mid latitudes of 30°-40° (Figure 1m, n and o). This concurs with satellite observations of highest particulate inorganic carbon (PIC; coccoliths) concentrations in surface waters at high latitudes (Balch et al., 2005; Iglesias-Rodríguez et al., 2002; Moore et al., 2012). Likewise, Jin et al. (2006) found high $CaCO_3$ export at 40° latitude using global nutrient and alkalinity observations and a biogeochemical model; however, the authors also found an equally large peak in export at the equator. A peak in export at the equator would not show up in Alk* if the simultaneous impacts of upwelling and export cancelled each other out. Sediment trap compilations (Berelson et al., 2007) and theoretical calculations (Sarmiento et al., 2002), indicate highest rain ratios (highest $CaCO_3$ export) towards the equator; however, there was no peak at mid latitudes.

*Alk** could also be used to validate biogeochemical models and improve model quantifications of $CaCO_3$ fluxes. The broad patterns in *Alk** should be reproduced in high-resolution global carbon cycle models if correctly formulated. The degree of agreement with *Alk** can be used as a check of the representations of ocean physics and $CaCO_3$ formation and dissolution. It may also be possible to improve methods for deducing $CaCO_3$ particle fluxes from ocean alkalinity data, by basing the inversion method on this method for *Alk**.

Finally, if ocean acidification leads to large reductions in calcification then an effect on ocean alkalinity may be detectable by 2040 (Ilyina et al., 2009). This may be more accurately determined using *Alk** rather than measured alkalinity as the method corrects for changes in

the water cycle (Huntington, 2006 and references therein) and productivity (e.g. Behrenfeld et al., 2006; Bopp et al., 2001; Gregg et al., 2003), which are also forecast to change. Time-series are often located close to the coast, because of ease of access, and consequently are frequently affected by river inputs. *Alk** is less variable than potential alkalinity in river-affected areas. This is because the standard deviation is reduced by the river correction (Table 2), making long term trends easier to detect (higher signal-to-noise ratio). This is illustrated in a simplistic way (Figure 9) in an example using data from the area of the Atlantic affected by the Amazon River outflow and an increase of 30 μmol kg^{-1} by 2040 (Ilyina et al. 2009). Following Ilyina et al. (2009), the trend is deemed to be detected when the magnitude of the change due to the trend exceeds the standard deviation of the data. According to this method (more sophisticated methods would be used in reality), the long-term trend is detectable by 2040 using *Alk** but not until 2060 using potential alkalinity.

Conclusions

In this study we derive a tracer for the ocean $CaCO_3$ cycle by subtracting the influences of other processes from the global surface alkalinity data, specifically (a) the hydrological cycle, (b) riverine discharge, and (c) the biological cycling of nutrients. On a regional scale, adjustment for the individual alkalinities of nearby large rivers was found to be particularly important in bringing anomalous values 'into line' in areas such as the tropical Atlantic Ocean, the Bay of Bengal and the Labrador Sea. The coherent geographic pattern revealed by our alkalinity tracer shows a constant value across the low latitudes of all major ocean basins, and well-defined, large magnitude increases of ~85 and ~110 μmol kg^{-1} towards the North Pacific and Southern Ocean respectively. The surface North Atlantic and North Atlantic Deep Water inherit low residual alkalinity from their source waters in the Atlantic subtropical gyres. Comparisons to nutrient distributions and calcium data strongly suggest that these

patterns in the residual alkalinity are caused by $CaCO_3$ cycling, i.e. upwelling mainly at high latitudes of deep water into which $CaCO_3$ has dissolved, and $CaCO_3$ export elsewhere that reduces *Alk** with increasing distance from the centers of upwelling. This residual alkalinity (*Alk**) therefore has considerable potential as a tracer of $CaCO_3$ cycling. This new tracer is likely to have many applications, including in quantification and localization of $CaCO_3$ export.

Acknowledgments

We thank all those who contributed to the collection, analysis, and synthesis of the GLODAP, CARINA, and PACIFICA databases. This study was financially supported by a NERC doctoral training grant to C. H. Fry (NE/K500926/1), and NERC IRF to M. P. Hain (NE/K00901X/1). We thank Dieter Wolf-Gladrow, Kitack Lee, Alex Poulton, Kevin Oliver and Mark Moore for helpful discussions.

References

Aminot, A., Kirkwood, D., 1995. Report on the results of the fifth ICES intercomparison exercise for nutrients in sea water. International Council for the Exploration of the Sea, Copenhagen, Denmark.

Amiotte Suchet, P., Probst, J.-K, Ludwig, W., 2003. Worldwide distribution of continental rock lithology: Implications for the atmospheric/soil CO_2 uptake by continental weathering and alkalinity river transport to the oceans. Global Biogeochem. Cycles, 17(2), 1038, doi:10.1029/2002GB001891.

Armstrong, R. A., Lee, C., Hedges, J.I., Honjo, S., Wakeham, S.G., 2002. A new, mechanistic model for organic carbon fluxes in the ocean based on the quantitative

association of POC with ballast minerals. Deep Sea Res., Part II, 49, 219–236, doi: 10.1016/S0967-0645(01)00101-1.

Balch, W.M., Gordon, H.R., Bowler, B.C., Drapeau, D.T., Booth, E.S., 2005. Calcium carbonate measurements in the surface global ocean based on Moderate-Resolution Imaging Spectroradiometer data. J. Geophys. Res. 110, C07001, doi:10.1029/2004JC002560.

Balch, W.M., Drapeau, D.T., Bowler, B.C., Lyczskowski, E., Booth, E.S., Alley, D., 2011. The contribution of coccolithophores to the optical and inorganic carbon budgets during the Southern Ocean Gas Exchange Experiment: New evidence in support of the "Great Calcite Belt" hypothesis. J. Geophys. Res. 116, C00F06, doi:10.1029/2011JC006941.

Barker, S., Higgins, J.A., Elderfield, H., 2003. The future of the carbon cycle: review, calcification response, ballast and feedback on atmospheric CO_2. Philos. Trans. A. Math. Phys. Eng. Sci. 361(1810), 1977–99, doi:10.1098/rsta.2003.1238.

Bates, N.R., Pequignet, A.C., Sabine, C.L., 2006. Ocean carbon cycling in the Indian Ocean: 1. Spatiotemporal variability of inorganic carbon and air-sea CO_2 gas exchange. Global Biogeochem. Cycles, 20(3), 1–13, doi:10.1029/2005GB002491.

Behrenfeld, M.J., O'Malley, R.T., Siegel, D.A., McClain, C.R., Sarmiento, J.L., Feldman, G.C., Milligan, A.J., Falkowski, P.G., Letelier, R.M., Boss, E.S., 2006. Climate-driven trends in contemporary ocean productivity. Nature, 444, 752-755, doi: 10.1038/nature05317.

Berelson, W.M., Balch, W.M., Najjar, R., Feely, R.A., Sabine, C., Lee, K., 2007. Relating estimates of $CaCO_3$ production, export, and dissolution in the water column to measurements of $CaCO_3$ rain into sediment traps and dissolution on the sea floor: A revised global carbonate budget. Global Biogeochem. Cycles, 21, GB1024, doi:10.1029/2006GB002803.

Bopp, L., Monfray, P., Aumont, O., Dufresne, J.L., Le Treut, H., Madec, G., Terray, L., Orr, J.C., 2001. Potential impact of climate change on marine export prodution. Global Biogeochem. Cycles, 15(1), 81-99, doi: 10.1029/1999GB001256.

de Boyer Montégut, C., Madec, G., Fischer, A.S., Lazar, A., Iudicone, D., 2004. Mixed layer depth over the global ocean: An examination of profile data and a profile-based climatology. J. Geophys. Res. 109, C12003, doi:10.1029/2004JC002378.

Bradshaw, A.L., Brewer, P.G., 1988. High precision measurements of alkalinity and total carbon dioxide in seawater by potentiometric titration. 2. Measurements on standard solutions. Mar. Chem. 24, 155-162, doi: 10.1016/0304-4203(88)90046-1.

Brewer, P.G., Goldman, J.C., 1976. Alkalinity changes generated by phytoplankton growth. Limnol. Oceanogr. 21(1), 108–117.

Brewer, P.G., Wong, G.T.F., Bacon, M.P., Spencer, D.W., 1975. An oceanic calcium problem? Earth Planet. Sci. Lett. 26, 81–87.

Cai, W.,Wang, Y., 1998. The chemistry, fluxes, and sources of carbon dioxide in estuarine waters of the Satilla and Altamaha Rivers, Georgia. Limnol. Oceanogr. 43(4), 657–668.

Cai, W.-J., Hu, X., Huang, W.-J., Jiang, L.-Q., Wang, Y., Peng, T.-H., Zhang, X., 2010. Alkalinity distribution in the western North Atlantic Ocean margins. J. Geophys. Res. 115, C08014, doi:10.1029/2009JC005482.

Cao, Z., Dai, M., 2011. Shallow-depth $CaCO_3$ dissolution: Evidence from excess calcium in the South China Sea and its export to the Pacific Ocean. Global Biogeochem. Cycles. 25, GB2019, doi:10.1029/2009GB003690.

Chen, C.T.A., 2002. Shelf- vs. dissolution-generated alklainity above the chemical lysocline. Deep Sea Res., Part II, 36, 5365-5375, doi: 10.1016/S0967-0645(02)00196-0.

Chung, S.N., Lee, K., Feely, R.A., Sabine, C.L., Millero, F.J., Wanninkhof, R., Bullister, J.L., Key, R.M., Peng, T.-H., 2003. Calcium carbonate budget in the Atlantic Ocean based on water column inorganic carbon chemistry. Global Biogeochem Cycles, 17(4), 1093, doi:10.1029/2002GB002001

Cooley, S.R., Yager, P.L., 2006. Physical and biological contributions to the western tropical North Atlantic Ocean carbon sink formed by the Amazon River plume. J. Geophys. Res. 111, C08018, doi:10.1029/2005JC002954.

Cooley, S.R., Coles, V.J., Subramaniam, A., Yager, P.L., 2007. Seasonal variations in the Amazon plume-related atmospheric carbon sink. Global Biogeochem. Cycles, 21, GB3014, doi:10.1029/2006GB002831.

Cooper, L.W., McClelland, J.W., Holmes, R.M., Raymond, P.A. , Gibson, J.J., Guay, C.K., Peterson, B.J., 2008. Flow-weighted values of runoff tracers ($\delta^{18}O$, DOC, Ba, alkalinity) from the six largest Arctic rivers. Geophys. Res. Lett. 35, L18606, doi:10.1029/2008GL035007.

Dickson, A. G., 1981. An exact definition of total alkalinity and a procedure for the estimation of alkalinity and total inorganic carbon from titration data. Deep. Res. 28A(6), 609–623.

Dickson, A.G., 2010. The carbon dioxide system in seawater : equilibrium chemistry and measurements, in: Riebesell, U. Fabry, V.J., Hansson, L., Gattuso, J.-P. (Eds.), Guide to best

practices for ocean acidification research and data reporting. Publications Office of the European Union, Luxembourg.

Dickson, A.G., Afghan, J.D., Anderson, G.C., 2003. Reference materials for oceanic CO_2 analysis: a method for the certification of total alkalinity. Mar. Chem. 80(2), 185-197, doi: 10.1016/S0304-4203(02)00133-0.

Dyrssen, D., Sillén, L.G., 1967. Alkalinity and total carbonate in sea water. A plea for p-T-independent data. Tellus A, 19(1), 113-121, doi: 10.1111/j.2153-3490.1967.tb01464.x.

Feely, R.A., Sabine, C.L., Lee, K., Millero, F.J., Lamb, M.F., Greeley, D., Bullister,J.L., Key, R.M., Peng, T.-H., Kozyr, A., Ono, T., Wong, C.S., 2002. In situ calcium carbonate dissolution in the Pacific Ocean. Global Biogeochem. Cycles, 16(4), 1144, doi:10.1029/2002GB001866.

Feely, R.A., Sabine, C.L., Lee, K., Berelson, W., Kleypas, J., Fabry, V.J., Millero, F.J., 2004. Impact of anthropogenic CO_2 on the $CaCO_3$ system in the oceans. Science, 305, 362–366, doi:10.1126/science.1097329.

Friis, K., Körtzinger, A., Wallace, D.W.R., 2003. The salinity normalization of marine inorganic carbon chemistry data. Geophys. Res. Lett. 30(2), 1085, doi:10.1029/2002GL015898.

Galy, A., France-Lanord, C., 1999. Weathering processes in the Ganges–Brahmaputra basin and the riverine alkalinity budget. Chem. Geol. 159, 31–60, doi:10.1016/S0009-2541(99)00033-9.

Goldman, J.G., Brewer, P.G., 1980. Effect of nitrogen source and growth rate on phytoplankton mediated changes in alkalinity. Limnol. Oceanogr. 25(2), 352-357.

Gran, G, 1952. Determination of the equivalence point in potentiometric titrations – Part II, Analyst, 77, 661-671.

Gregg, W.W., Conkright, M.E., Ginoux, P., O'Reilly, J.E., Casey, N.W., 2003. Ocean primary production and climate: Global decadal changes. Geophys. Res. Lett. 30(15), 1809, doi: 10.1029/2003GL016889.

Hain, M.P., Sigman, D.M., Haug, G.H., 2010. Carbon dioxide effects of Antarctic stratification, North Atlantic Intermediate Water formation, and subantarctic nutrient drawdown during the last ice age: Diagnosis and synthesis in a geochemical box model. Global Biogeochem. Cycles, 24, GB4023, doi: 10.1029/2010GB003790.

Holligan, P.M., Robertson, J.E., 1996. Significance of ocean carbonate budgets for the global carbon cycle. Global Change Biol. 2(2), 85-95, doi: 10.1111/j.1365-2486.1996.tb00053.x.

Hu, X., Cai, W.J., 2011. An assessment of ocean margin anaerobic processes on oceanic alkalinity budget, Global Biogeochem. Cycles, 25, GB3003, doi:10.1029/2010GB003859.

Huntington, T.G., 2006. Evidence for intesification of the global water cycle: Review and synthesis. J. Hydrol. 319, 83-95, doi: 10.1016/j.jhydrol.2005.07.003.

Iglesias-Rodríguez, M.D., Brown, C.W., Doney, S.C., Kleypas, J., Kolber, D., Kolber, Z., Hayes, P.K., Falkowski, P.G., 2002. Representing key phytoplankton functional groups in ocean carbon cycle models: Coccolithophorids. Global Biogeochem. Cycles, 16(4), 1100, doi:10.1029/2001GB001454.

Ilyina, T., Zeebe, R.E., Maier-Reimer, E., Heinze, C., 2009. Early detection of ocean acidification effects on marine calcification. Global Biogeochem. Cycles, 23, GB1008, doi:10.1029/2008GB00327.

Jiang, Z.-P., Tyrrell, T., Hydes, D.J., Dai, M.,Hartman, S., 2014. Variability of alkalinity and alkalinity-salinity relationship in the tropical and subtropical surface ocean. Global Biogeochem. Cycles, 28(7), 729-742, doi: 10.1002/2013GB004678..

Jin, X., Gruber, N., Dunne, J.P., Sarmiento, J.L., Armstrong, R.A., 2006. Diagnosing the contribution of phytoplankton functional groups to the production and export of particulate organic carbon, $CaCO_3$, and opal from global nutrient and alkalinity distributions. Global Biogeochem. Cycles, 20, GB2015, doi:10.1029/2005GB002532.

Kang, Y., Pan, D., Bai, Y., He, X., Chen, X., Chen, C.-T.A., Wang, D., 2013. Areas of the global major river plumes. Acta Oceanol. Sin. 32(1), 79–88, doi:10.1007/s13131-013-0269-5.

Key, R.M., Tanhua, T., Olsen, A., Hoppema, M., Jutterström, S., Schirnick, C., van Heuven, S., Kozyr, A., Lin, X., Velo, A., Wallace, D.W.R., Mintrop, L., 2010. The CARINA data synthesis project: introduction and overview. Earth Syst. Sci. Data, 2, 105–121, doi:10.5194/essd-2-105-2010.

Key, R., Kozyr, A., Sabine, C., Lee, K., Wanninkhof, R., Bullister, J.L., Feely, R.A., Millero, F.J., Mordy, C., Peng, T.-H., 2004. A global ocean carbon climatology: Results from Global Data Analysis Project (GLODAP). Global Biogeochem. Cycles, 18, GB4031, doi: 10.1029/2004GB002247.

Klaas, C., Archer, D.E., 2002. Association of sinking organic matter with various types of mineral ballast in the deep sea: Implication for the rain ratio. Global Biogeochem. Cycles, 16(4), 1116, doi: 10.1029/2001GB001765.

Kwon, E.Y., Primeau, F., Sarmiento, J.L., 2009. The impact of remineralization depth on the air-sea carbon balance. Nat. Geosci. 2, 630-635, doi: 10.1038/ngeo612.

Lee, K., 2001. Global net community production estimated from the annual cycle of surface water total dissolved inorganic carbon. Limnol. Oceanogr. 46(6), 1287-1297, doi: 10.4319/lo.2001.46.6.1287.

Lee, K., Tong, L.T., Millero, F.J., Sabine, C.L., Dickson, A.G., Goyet, C., Park, G.-H., Wanninkhof, R., Feely, R.A., Key, R.M., 2006. Global relationships of total alkalinity with salinity and temperature in surface waters of the world's oceans. Geophys. Res. Lett. 33, L19605, doi:10.1029/2006GL027207.

Lozier, M.S., 2012. Overturning in the North Atlantic. Ann. Rev. Mar. Sci. 4, 291-315, doi: 10.1146/annurev-marine-120710-100740.

Millero, F.J., Dickson, A.G., Eischeid, G., Goyet, C., Guenther, P., Johnson, K.M., Key, R.M., Lee, K., Purkerson, D., Sabine, C.L., Schottle, R.G., Wallace, D.W.R., Lewis, E., Winn, C.D., 1998a. Assessment of the quality of the shipboard measurements of total alkalinity on the WOCE Hydrographic Program Indian Ocean CO_2 survey cruises 1994–1996. Mar. Chem. 63, 9–20, doi:10.1016/S0304-4203(98)00043-7.

Millero, F.J., Lee, K., Roche, M., 1998b. Distribution of alkalinity in the surface waters of the major oceans. Mar. Chem. 60, 111–130, doi:10.1016/S0304-4203(97)00084-4.

Milliman, J.D., Troy, P.J., Balch, W.M., Adams, A.K., Li, Y.-H., Mackenzie, F.T., 1999. Biologically mediated dissolution of calcium carbonate above the chemical lysocline? Deep Sea Res., Part I. 46, 1653–1669, doi:10.1016/S0967-0637(99)00034-5.

Moore, T.S., Dowell, M.D., Franz, B.A., 2012. Detection of coccolithophore blooms in ocean color satellite imagery: A generalized approach for use with multiple sensors. Remote Sens. Environ. 117, 249–263, doi:10.1016/j.rse.2011.10.001.

Ohno, Y., Iwasaka, N., Kobashi, F., Sata, Y., 2009. Mixed layer depth climatology of the North Pacific based on Argo observations. J. Oceanogr. 65(1), 1-16, doi: 10.1007/s10872-009-0001-4.

Olson, E.J., Chen, C.T.A., 1982. Interference in the determination of calcium in seawater. Limnol. Oceanogr. 27(2), 375-380.

Pardo, P.C., Vázquez-Rodríguez, M., Pérez, F.F., Rios, A.F., 2011. CO_2 air-sea disequilibrium and preformed alkalintiy in the Pacific and Indian oceans calculated from subsurface layer data. J. Mar. Sys. 84, 67-77, doi: 10.1016/j.jmarsys.2010.08.006.

Pavlova, G.Y., Tishchenko, P.Y., Nedashkovskii, A.P., 2008. Distribution of alkalinity and dissolved calcium in the Sea of Okhotsk. Oceanology, 48(1), 23–32, doi:10.1134/S0001437008010049.

Perkin, R.G., Lewis, E., 1980. The practical salinity scale 1978: Fitting the data. 5(1), 9-16, doi: 10.1109/JOE.1980.1145441.

Postma, H., 1964. The exchange of oxygen and carbon dioxide between the ocean and the atmosphere. Neth. J. Sea Res. 2(2), 258–283.

Poulton, A.J., Sanders, R., Holligan, P.M., Stinchcombe, M.C., Adey, T.R., Brown, L., Chamberlain, K., 2006. Phytoplankton mineralization in the tropical and subtropical Atlantic Ocean. Global Biogeochem. Cycles, 20, GB4002, doi:10.1029/2006GB002712.

Rubin, S.I., Key, R.M., 2002. Separating natural and bomb-produced radiocarbon in the ocean: The potential alkalinity method. Global Biogeochem. Cycles, 16(4), 1105, doi:10.1029/2001GB001432.

Rysgaard, S., Søgaard, D.H., Cooper, M., Pućko, M., Lennert, K., Papakyriakou, T.N., Wang, F., Geilfus, N.X., Glud, R.N., Ehn, J., McGinnis, D.F., Attard, K., Sievers, J., Deming, J.W., Barber, D., 2013. Ikaite crystal distribution in winter sea ice and implications for CO_2 system dynamics. Cryosphere. 7, 707–718, doi:10.5194/tc-7-707-2013.

Rysgaard, S., Glud, R.N., Lennert, K., Cooper, M., Halden, N., Leakey, R.J.G., Hawthorne, F.C., Barber, D., 2012. Ikaite crystals in melting sea ice – implications for pCO_2 and pH levels in Arctic surface waters. Cryosphere, 6, 1–8, doi:10.5194/tc-6-1-2012.

Sabine, C.L., Key, R.M., Feely, R.A., Greeley, D., 2002. Inorganic carbon in the Indian Ocean: Distribution and dissolution processes. Global Biogeochem. Cycles, 16(4), 1067, doi:10.1029/2002GB001869.

Sarmiento, J.L., Dunne, J., Gnanadesikan, A., Key, R.M., Matsumoto, K., Slater, R., 2002. A new estimate of the $CaCO_3$ to organic carbon export ratio. Global Biogeochem. Cycles, 16(4), 1107, doi:10.1029/2002GB001919.

Sarmiento, J.L., Gruber, N., Brzezinski, M.A., Dunne, J.P., 2004. High-latitude controls of thermocline nutrients and low latitude biological productivity. Nature, 427, 56–60, doi:10.1038/nature02204.1.

Schlitzer, R., 2000. Applying the Adjoint Method for Biogeochemical Modeling: Export of Particulate Organic Matter in the World Ocean, in: Kasibhatla, P., Heimann, M., Rayner, P., Mahowald, N., Prinn, R.G., Hartley, D.E. (Eds.), Inverse Methods in Global Biogeochemical Cycles. AGU, Washington D.C., pp. 107–124.

Talley, L.D., Reid, J.L., Robbins, P.E., 2003. Data-Based Meridional Overturning Streamfunctions for the Global Ocean. J. Clim. 16, 3213–3226, doi: 10.1175/1520-0442(2003)016<3213:DMOSFT>2.0.CO;2.

Taylor, J.R., 1982. An introduction to error analysis: The study of uncertainties in physcial measurements. University Science Books, Mill Valley, C.A.

Toggweiler, J.R., Samuels, B., 1995. Effect of Drake Passage on the global thermohaline circulation. Deep Sea Res. I, 42(4) 477-500, doi: 10.1016/0967-0637(95)00012-U.

Tsunogai, S., Yamahata, H., Kudo, S., Saito, O., 1973. Calcium in the Pacific Ocean. Deep Sea Res. 20, 717-726.

Vázquez-Rodríguez, M., Padin, X.A., Pardo, P.C., Ríos, A.F., Pérez, F.F., 2012. The subsurface layer reference to calculate preformed alkalinity and air-sea CO_2 disequilibrium in the Atlantic Ocean. J. Mar. Sys. 94, 52-63, doi: 10.1016/j.jmarsys.2011.10.008.

de Villiers, S., 1998. Excess dissolved Ca in the deep ocean: a hydrothermal hypothesis. a Earth Planet. Sci. Lett. 164, 627-741, doi: 10.1016/S0012-821X(98)00232-5.

de Villiers, S., Nelson, B.K., 1999. Detection of low-temperature hydrothermal fluxes by seawater Mg and Ca anomalies. Science, 285, 721-723, doi: 10.1126/science.285.5428.721.

Wolf-Gladrow, D.A., Zeebe, R.E., Klaas, C., Körtzinger, A., Dickson, A.G., 2007. Total alkalinity: The explicit conservative expression and its application to biogeochemical processes. Mar. Chem. 106(1-2), 287–300, doi:10.1016/j.marchem.2007.01.006.

Wong, G.T.F., 1979. Alkalinity and pH in the southern Chesapeake Bay and the James River estuary. Limnol. Oceanogr. 24(5), 970–977.

Figure 1. The distribution of alkalinity (µmol kg^{-1}) and normalized alkalinity (µmol kg^{-1}) in each ocean basin. a,b, and c show the observed alkalinity with the colors indicating the salinity from 32 to 37. d,e, and f show salinity normalized alkalinity (Alk_1) with red points indicating values more than 20 µmol kg^{-1} from the 5°of latitude running mean. g,h and i are Alk_2, where rivers are included for each basin. j,k, and l show Alk_3, where the biological uptake of nutrients is also included, for each basin. m,n and o show *Alk**. Note the different y-axis scale on the first row of plots.

Figure 2. Salinity versus (a) alkalinity (µmol kg^{-1}) and (b) normalized alkalinity (Alk_1, µmol kg^{-1}) in the global surface ocean.

Figure 3. Salinity-normalized alkalinity (Alk_1, µmol kg^{-1}) gridded to 5° latitude and longitude in the surface ocean.

Figure 4. Indian Ocean alkalinity (µmol kg^{-1}) as a function of latitude following salinity-normalization using equation 4 with Alk_r = 1107 µmol kg^{-1} in the Bay of Bengal area (north of 5°N and between 80°E and 94°E).

Figure 5. Normalized alkalinity anomaly ($Alk^* = Alk_3$ - 2300, µmol kg^{-1}) along the GLODAP section illustrated in the insert.

Figure 6. Surface distribution of *Alk** µmol kg^{-1} (a,b,c), nitrate µmol kg^{-1} (d,e,f), phosphate µmol kg^{-1} (g,h,i), silicate µmol kg^{-1} (j,k,l) in each ocean basin from the GLODAP, CARINA and PACIFICA databases.

Figure 7. The mixing relationship between salinity and alkalinity when calcification also takes place. When an ocean body (A) mixes with river water (R) and calcification occurs, the final alkalinity-salinity relationship will depend on whether the calcification occurred before (A to b to c) or after (A to d to e) mixing.

Figure 8. Representation of Atlantic Basin circulation and fluxes. $Alk^*_{S.Oc}$ and Alk^*_{gyre} are the alkalinity anomalies of the Southern Ocean and Atlantic gyre respectively. F_{ekman} is the surface Ekman flux in the Southern Ocean, F_{NADW} the NADW flux and Q_{Atl} is the flux of alkalinity leaving the gyre through $CaCO_3$ precipitation. Equatorial upwelling and mixing across the thermocline are omitted as they do not contribute to the first order Alk* pattern.

Figure 9. Modelled *Alk** in an area of the ocean affected intermittently by the Amazon River outflow. Alk* is shown both with river adjustment included (top) and without it (bottom). The simulated data was produced using a random number generator to produce random numbers from a normal distribution with a standard deviation (dashed line) of 16.5 µmol kg^{-1} (top panel) and 25.6 µmol kg-1 (bottom panel). These standard deviations are the standard deviations of the actual Alk* values in the region affected by the Amazon (Table 2), depending on whether adjusted to take account of Amazon alkalinity or not. An alkalinity increase over time of 30 µmol kg^{-1} from 2010 until 2040 was added to the random numbers to produce the simulated data. Data sampling frequency of 30 days.

Figure 1

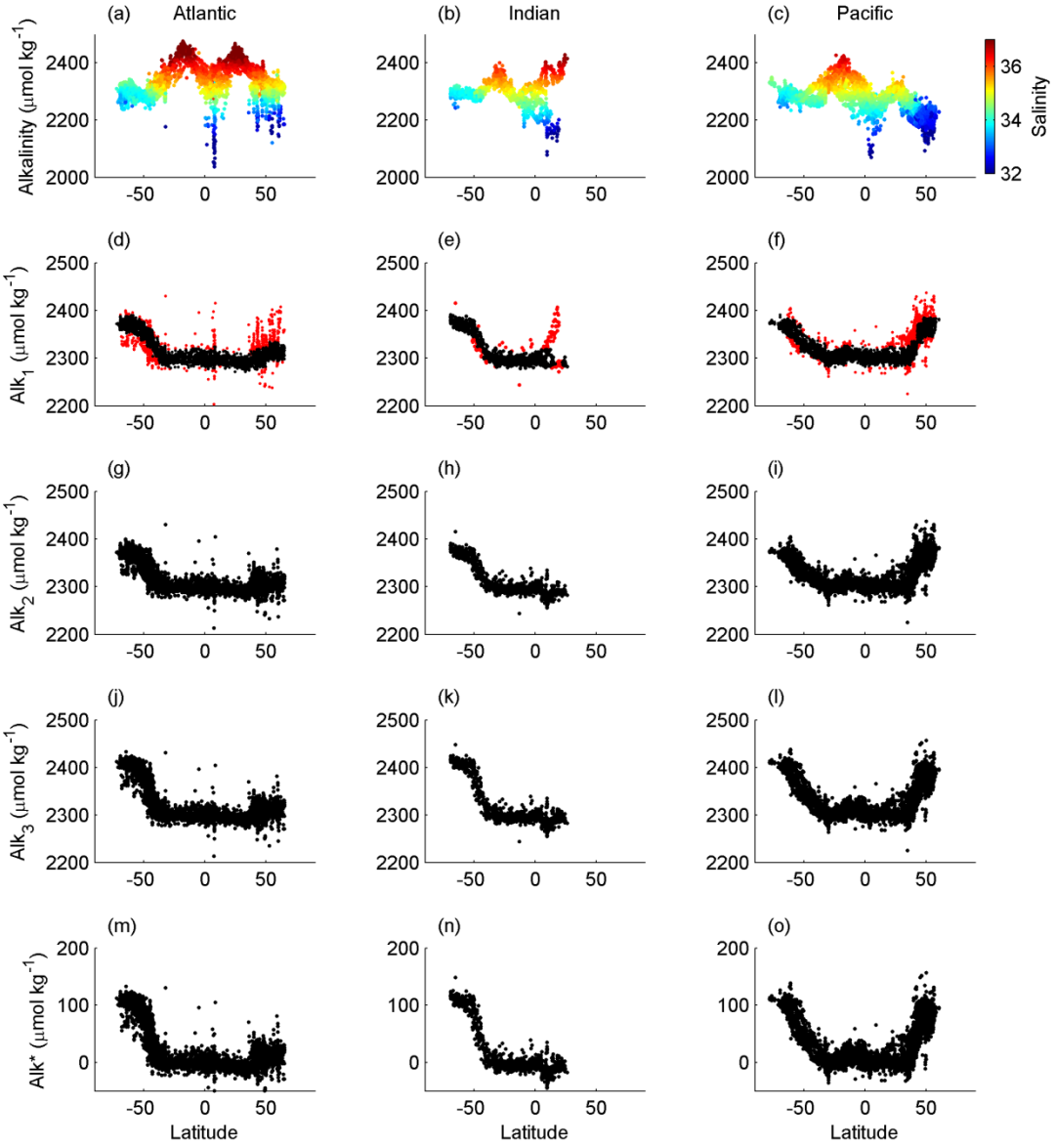

Figure 2

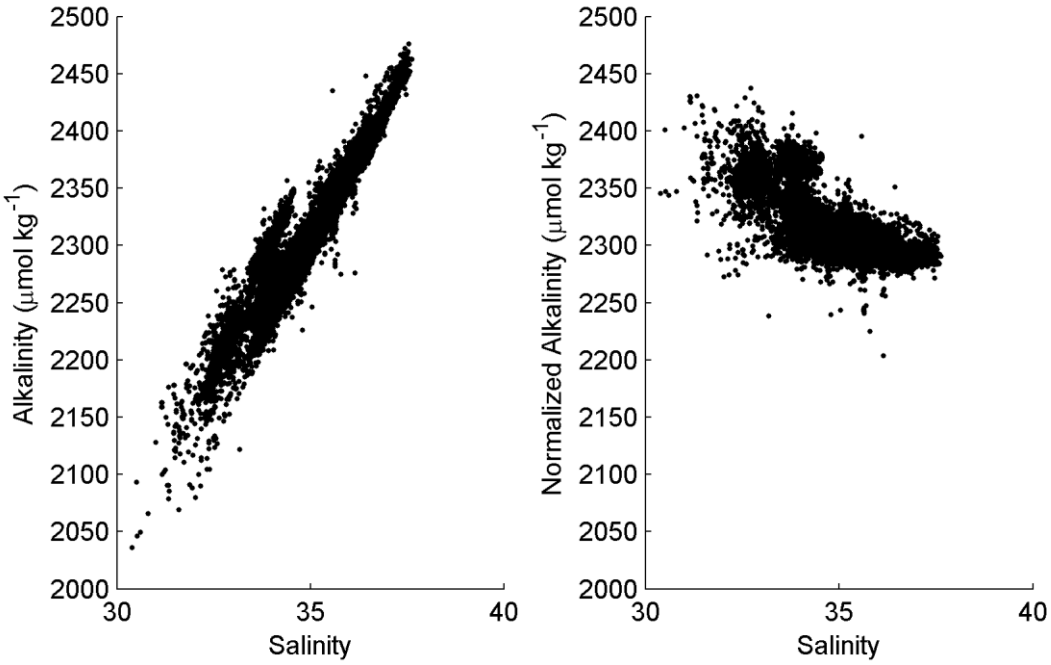

Figure 3

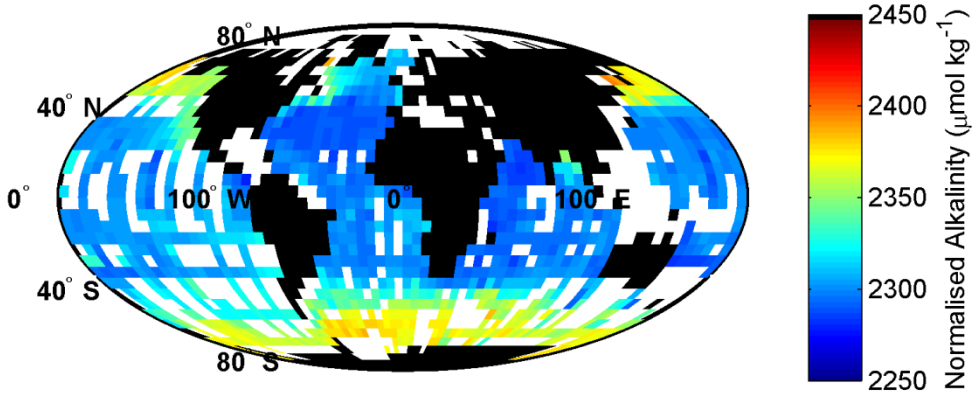

Figure 4

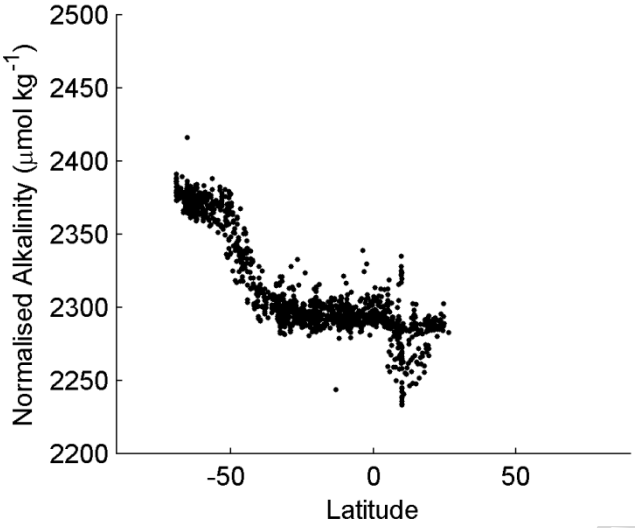

Figure 5

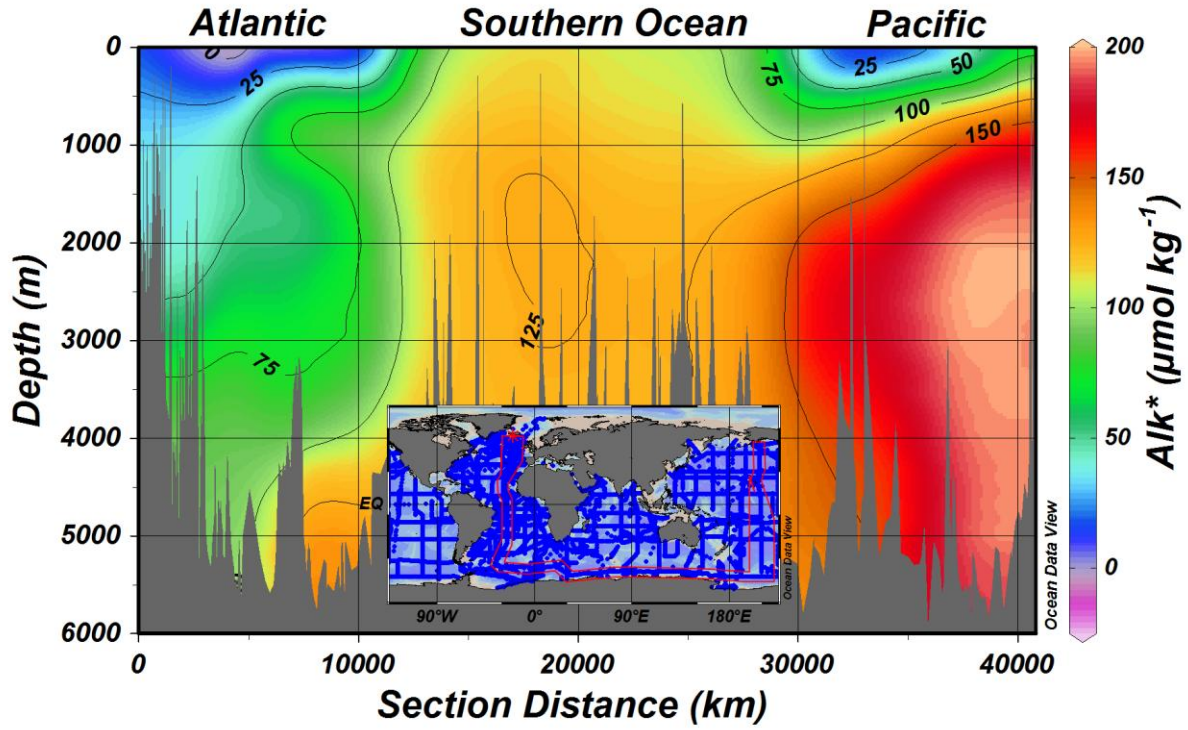

Figure 6

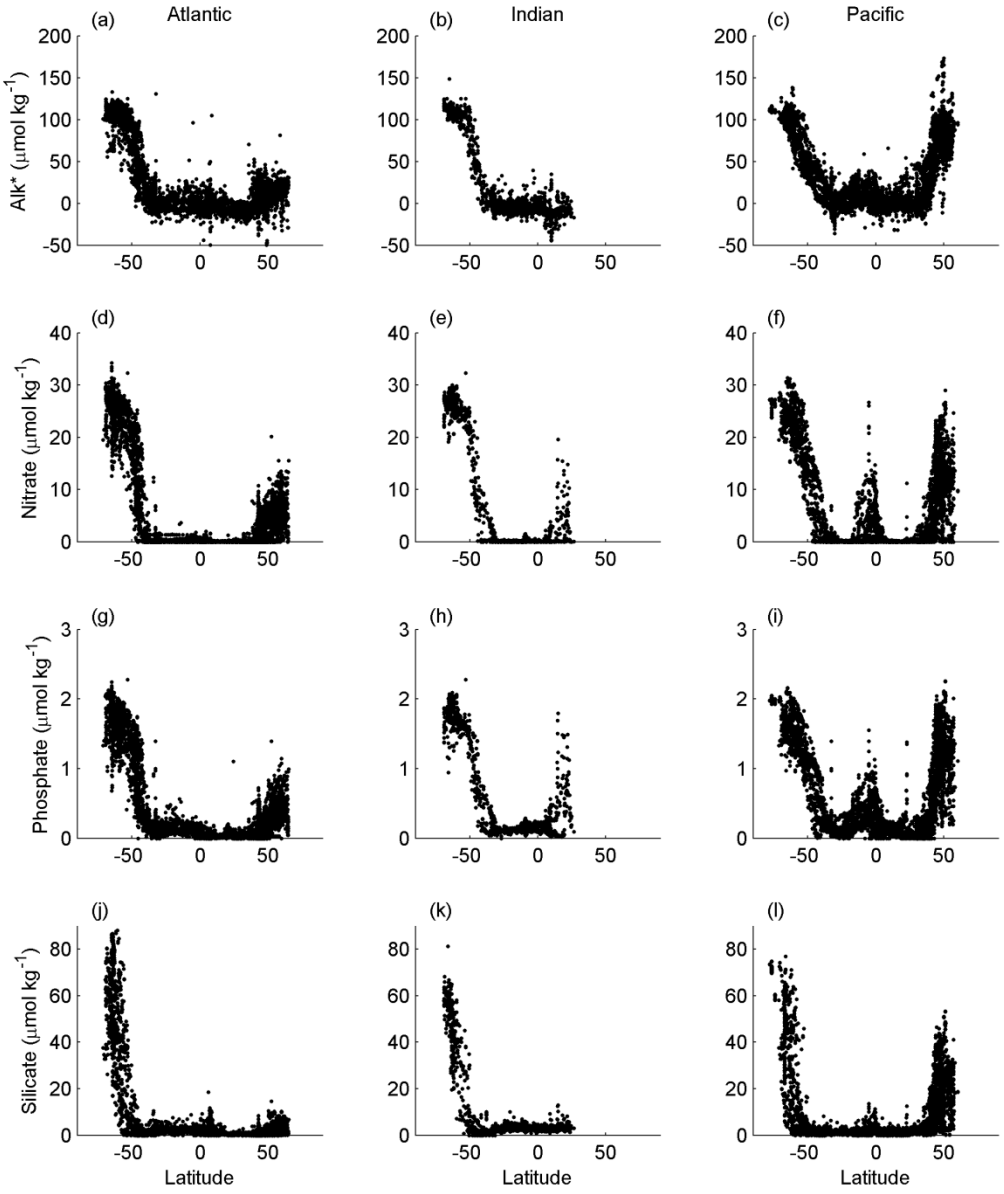

Figure 7

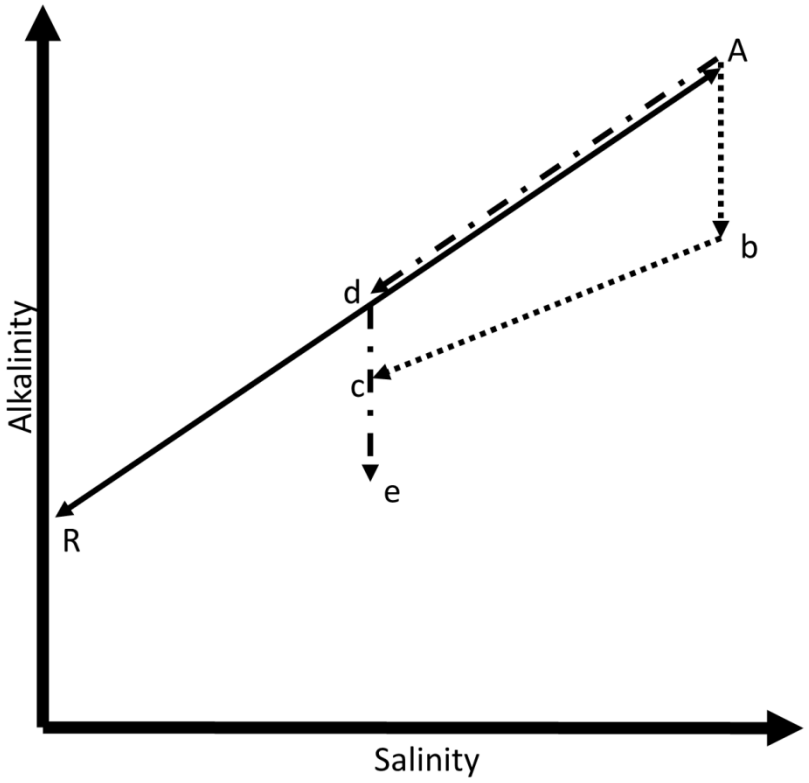

Figure 8

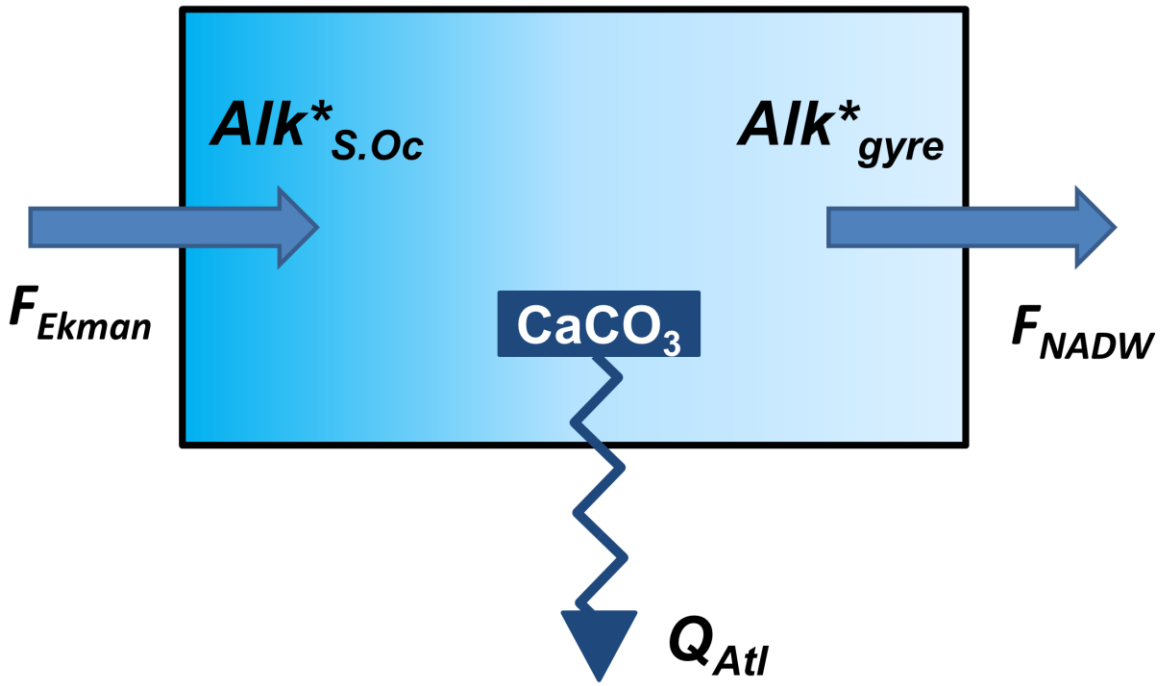

Figure 9

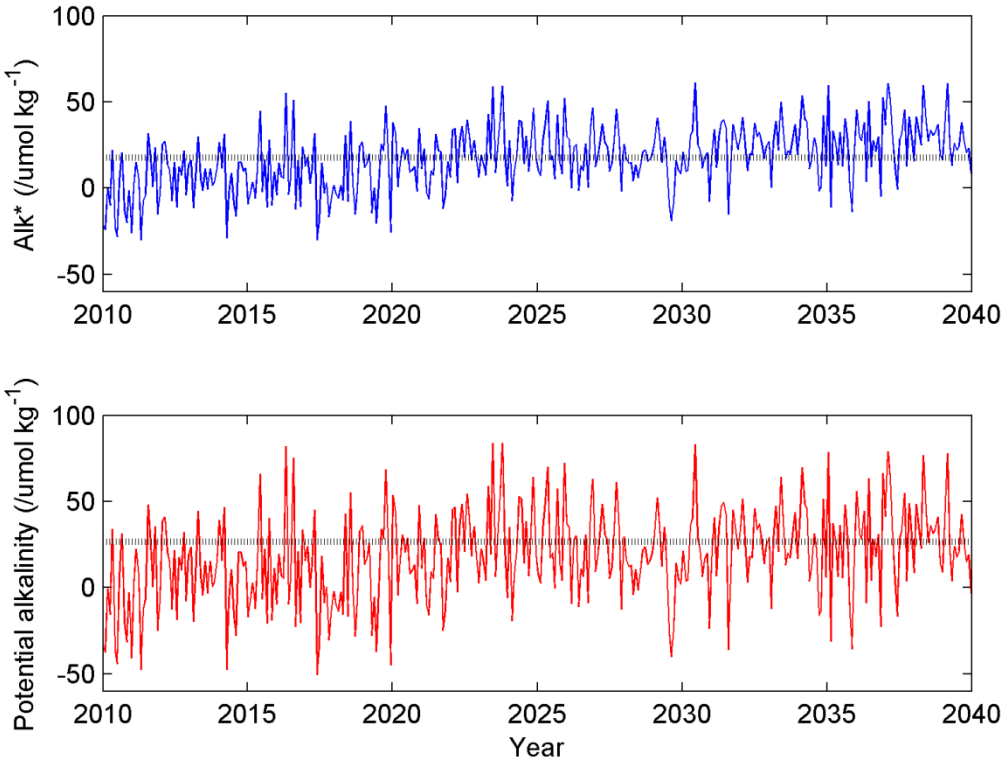

Table 1. Variability in alkalinity and nutrients[a]

	Alkalinity				Nutrients	
	Initial	After correction				
		Evaporation Precipitation	Riverine Input	Biological Growth and remineralization	Nitrate	Phosphate	Silicate
Atlantic	0.17	0.14	0.13	0.095	0.064	0.077	0.067
Indian	0.11	0.095	0.080	0.071	0.066	0.086	0.060
Pacific	0.17	0.14	0.14	0.11	0.097	0.10	0.065

[a]Calculated as the average of the standard deviations in the 5° latitude bins, divided by the range in the mean values of the 5° latitude bins. Calculations are made for each ocean basin after each cumulative stage has been taken into account, and for each macronutrient.

Table 2. River Alkalinity (Alk_r) Corrections

Area Name	Ocean Basin	Area boundaries	Alk_r (µmol kg^{-1})
Amazon plume	Atlantic	5°N<Latitude<10°N, Longitude<-45°E	300
Labrador Sea	Atlantic	Latitude>40°N, Longitude<-30°E	1100
Bay of Bengal	Indian	Latitude>5°N, 80°E<Longitude<94°E	840

Table 3. Estimates of Annual Production of Particulate Inorganic Carbon in the Atlantic Ocean Basin

	Pg PIC yr^{-1}
Lee (2001)	0.43
Poulton et al. (2006)	0.69[a]
Berelson et al. (2007)	0.11-0.35
Our estimate	0.03

[a]Flux estimate from data collected during northern hemisphere spring (southern hemisphere autumn).

Highlights

- Development of a alkalinity-based tracer of $CaCO_3$ cycling in the surface ocean
- Tracer exhibits spatial features not apparent in alkalinity distributions
- Difference of ~110 µmol kg^{-1} between low latitudes and the Southern Ocean
- Difference of ~85 µmol kg^{-1} between low latitudes and the subarctic North Pacific